Geomechanics and Engineering, *Vol. 43, No. 3 (2025) 213-226*
https://doi.org/10.12989/gae.2025.43.3.213

Cr^{3+}-crosslinked xanthan gum hydrogels for enhancing penetration efficiency and post-installation pullout resistance of bioinspired piles

Suhyuk Park[1a], Saebom Kim[1b], Su-Choel Kim[2c] and Ilhan Chang*[1]

[1]*Department of Civil Systems Engineering, Ajou University, Suwon 16499, Republic of Korea*
[2]*Civil Engineering Headquarters, Kumho E&C, Seoul 03161, Republic of Korea*

(*Received September 27, 2025, Revised October 13, 2025, Accepted October 17, 2025*)

Abstract. The use of biopolymer hydrogels for bioinspired piles is emerging as a sustainable approach to enhance penetration efficiency and ensure pile stability after installation. Xanthan gum (XG) hydrogels possess shear-thinning properties, which reduce penetration resistance under high shear strain conditions. However, their limited durability under wet conditions restricts their field application. To address this, this study introduces trivalent chromium (Cr^{3+}) crosslinked XG and investigates the mechanical performance enhancement of treated soils and piles. Rheological tests revealed that both XG and Cr–XG hydrogels exhibited shear-thinning behavior with increasing shear rate, whereas Cr^{3+} crosslinking significantly increased yield stress and flow point, thereby enhancing structural stability after gelation. Direct and interface shear-test results showed that XG concentration and Cr^{3+} addition significantly increased cohesion and interface adhesion. Laboratory-scale pile-penetration tests demonstrated that XG-hydrogel injection reduced end bearing and skin friction during penetration, improving installation efficiency. The pile treated with 1.0% Cr–XG exhibited the highest pullout resistance post-installation. These results demonstrate the potential of the Cr–XG 1.0% hydrogel to simultaneously improve penetration efficiency and post-installation stability, presenting a bioinspired strategy for sustainable pile-foundation design.

Keywords: bioinspired pile; Cr^{3+}-induced XG crosslinking; penetration; pullout resistance; xanthan gum (XG)

1. Introduction

Pile foundations transfer structural loads to deep, stiff soil layers when the surface soil is weak (Nguyen *et al.* 2017). However, a large penetration resistance during pile driving can lead to increased equipment wear (Quanjie *et al.* 2024), noise, and vibration (Göttsche *et al.* 2015). The pile bearing capacity after installation must also be assessed. Pullout resistance tests on the piles are used to evaluate whether the pile structure has been properly installed. These tests are commonly employed to assess the soil–pile interface behavior and ensure structural stability (Das and Sivakugan 2018). Therefore, the key challenges in pile foundation design are reducing the penetration resistance to improve workability and maintaining or enhancing the bearing capacity after pile installation.

The recent increase in carbon-dioxide emissions has led to a growing demand in geotechnical engineering for sustainable, low-carbon construction methods (Chang *et al.* 2019), and bio-inspired geotechnical engineering is gaining attention as an alternative to conventional soil stabilization (Zhang *et al.* 2023, Zivari *et al.* 2023, Jerez Lazo *et al.* 2024, Sierra *et al.* 2024, Zhang *et al.* 2024). Bioinspired geotechnics implements soil–structure interfaces by mimicking biological systems such as animals, plants, or eco-friendly hydrogels to achieve friction reduction, lubrication, and surface roughness (Martinez *et al.* 2021, Zhang *et al.* 2023, Park *et al.* 2024b). Among these methods, biopolymer-based soil treatment has recently been the focus of extensive research. Xanthan gum (XG) is a microbial biopolymer that enhances soil strength (Chang *et al.* 2015, Wan *et al.* 2024), reduces hydraulic conductivity (Chang *et al.* 2023, Zhang *et al.* 2024), and reduces soil erosion (Dai *et al.* 2023, Kwon *et al.* 2023b). Notably, XG hydrogels exhibit shear-thinning properties, where the viscosity decreases with increasing shear strain or rate, facilitating lubrication or slippage (Chantaro *et al.* 2013, Liu and Yao 2015). Based on these characteristics, XG has recently been applied in various fields within biogeotechnics to reduce friction (Chang *et al.* 2015, Kim *et al.* 2023, Kwon *et al.* 2023a, Lee *et al.* 2024). However, XG has limitations such as strength degradation due to repeated wetting–drying cycles, difficulty in ensuring stable strength in wet conditions, and sensitivity to water content (Casas *et al.* 2000, Lee *et al.* 2022, Chen *et al.* 2024).

To address these drawbacks, crosslinking techniques that enhance the XG performance have recently been studied. Specifically, trivalent chromium (Cr^{3+}) and crosslinked XG (Cr–XG) hydrogels can achieve time-dependent gelation (Lee *et al.* 2023a), high shear strength and unconfined compressive strength when combined with soil, and durability in water (Bang *et al.* 2024, Bang *et al.* 2025). Furthermore, strength degradation owing to repeated immersion is insignificant compared to a single treatment,

*Corresponding author, Professor
E-mail: ilhanchang@ajou.ac.kr
[a]Ph.D. student
[b]Master student
[c]Project manager

ISSN: 2005-307X (Print), 2092-6219 (Online)

and unlike an XG single treatment, Cr–XG can maintain hydrogel strength under wet conditions. However, the interface shear behavior between Cr–XG-treated soils and structures and the effectiveness of the Cr–XG hydrogel on reducing penetration resistance and improving pullout resistance during pile construction have not been sufficiently studied.

This study investigates the feasibility of applying a Cr–XG hydrogel to pile foundations to reduce penetration resistance during installation and enhance post-installation pullout capacity. Direct and interface shear tests are conducted to determine the shear and interface shear parameters of each soil type. Laboratory-scale pile-penetration tests assess installation efficiency using the penetration resistances of the pile components (tip and shaft) and associated load-settlement responses. Post-installation pullout tests evaluate whether sufficient adhesion is maintained post-installation by utilizing the skin friction occurring at the interface between the pile and Cr–XG soils. Based on the obtained results, this study investigates the impact of Cr–XG treatment on the overall constructability and bearing capacity during pile installation, providing an experimental foundation and valuable insights for bioinspired sustainable pile design.

2. Materials and methods

2.1 Soils and materials

2.1.1 Soil: Jumunjin sand

Jumunjin natural sand was used in this study. The specific gravity of the soil was determined to be 2.65 according to ASTM D854 (ASTM 2000). The D_{10}, D_{30}, and D_{60} sizes of the soil were determined through sieve analysis to be 0.62 mm, 1.21 mm, and 1.50 mm, respectively. The coefficients of uniformity (C_u) and curvature (C_c) were 2.42 and 1.57, respectively. Based on the Unified Soil Classification System (USCS) classification, the soil was classified as a poorly graded sand (SP). The maximum and minimum dry densities of the soil were determined to be 17.9 kN/m³ and 14.6 kN/m³, respectively, according DIN 18126 (DIN 1996), corresponding to a void ratio range (0.48–0.78). A detailed particle size distribution curve and the soil properties are presented in Fig. 1.

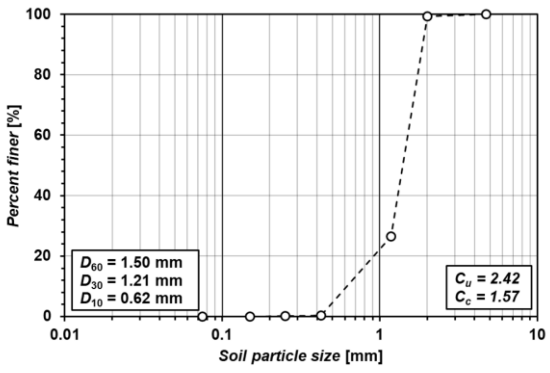

C_u	C_c	G_s	USCS	$\gamma_{d,max}$	$\gamma_{d,min}$
2.42	1.57	2.65	SP	17.9 kN/m³	14.6 kN/m³

Fig. 1 Particle size distribution curve and soil properties

2.1.2 Biopolymer: Xanthan gum

Research-grade Xanthan gum (CAS No. 11138-66-2, Sigma-Aldrich, USA), an anionic heteropolysaccharide produced by *Xanthomonas campestris*, was used in this study. Xanthan gum (XG) is a biodegradable and environmentally benign biopolymer (Katzbauer 1998) that is widely used as a soil stabilizer in geotechnical engineering (Chang *et al.* 2015, Kim *et al.* 2025). When dissolved in water, XG molecules form a three-dimensional hydrogel network with high viscosity owing to chain entanglement and hydrogen bonding, even at low concentrations (Mali *et al.* 2023). The interparticle coating (Lee and Chang 2025), pore-filling, and bridging mechanisms of XG hydrogels have been shown to reduce hydraulic conductivity (Tran *et al.* 2019) and enhance shear strength (Chang and Cho 2019). Furthermore, XG hydrogels exhibit shear-thinning properties (Comba and Sethi 2009, Zhong *et al.* 2013); therefore, the viscosity of the solution decreases as the shear rate increases. This characteristic has been recently used in various materials to reduce friction (Lee *et al.* 2021). This study investigates the effect of XG on reducing resistance and increasing workability during pile driving.

2.1.3 Trivalent chromium for crosslinked Xanthan gum

Chromium (III) nitrate nonahydrate ($Cr(NO_3)_3 \cdot 9H_2O$; CAS: 7789-02-8, Sigma-Aldrich, USA) in crystal form was used for crosslinking with XG. Cr^{3+} ions (Cr) formed coordinate bonds with the carboxyl (-COOH) and hydroxyl (-OH) groups of XG, creating a three-dimensional crosslinked network (Cr–XG) (Mali *et al.* 2023). This reaction produces stronger crosslinks with trivalent ions than with divalent ions (crosslinked XG; Cr–XG). It exhibits high reactivity with XG over a wide pH range (Ahmad *et al.* 2015) to form Cr–XG gelation within an appropriate curing time (Prud'homme *et al.* 1983, Lund *et al.* 1988). Cr^{3+} is an essential trace element for animals and humans and has the advantage of a lower toxicity than hexavalent chromium (Cr^{6+}) (Baruthio 1992). This study evaluates the effect of Cr–XG on the pullout resistance of piles after installation.

2.2 Preparation of Cr–XG hydrogels and soil samples

XG hydrogels were prepared by mixing XG powder and deionized water at two mass ratios (m_x/m_w = 2.5 and 5.0%). This was performed using a hand mixer (capacity: 20,000 rpm) for 1 min to obtain a homogeneous hydrogel. For Cr–XG, research-grade chromium (III) nitrate nonahydrate (Cr^{3+}) was added to the hydrogel after the initial mixing of XG and water. The Cr/XG mass ratio was set to 30%, and the optimal ratio was established based on prior literature (Lee *et al.* 2023a). After adding crystal-type Cr^{3+}, the mixture was post-mixed for 1 min to obtain a uniformly crosslinked hydrogel.

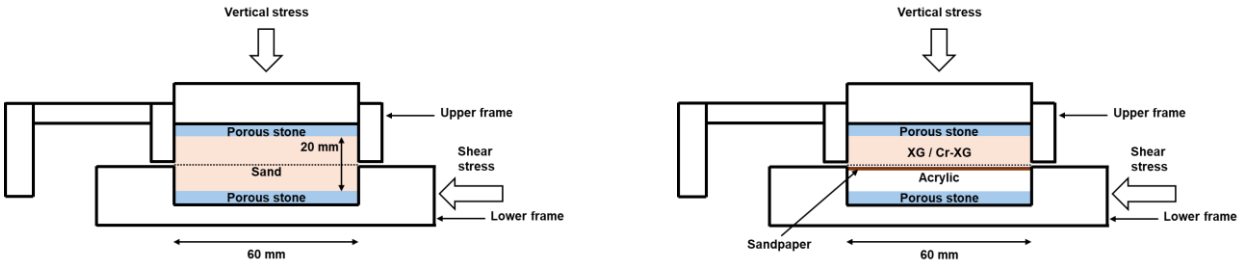

(a) Direct shear test (b) Interface shear test

Fig. 2 Schematics of shear tests of sand and XG/Cr–XG

The prepared XG and Cr–XG hydrogels were mixed with Jumunjin sand to prepare the soil specimens. For the XG- and Cr–XG-treated soils, the soil-to-XG ratios (m_x/m_s) were set to 0.5% and 1.0%, and Cr/XG was set to 30% before mixing. The dry unit weight of the soil samples was 16.3 kN/m³, corresponding to a relative density of 57%. The prepared specimens were cured at 20°C for three days.

2.3 Rheological tests

The rheological properties of the XG and Cr–XG hydrogels were characterized at room temperature using a controlled-stress rheometer (MCR 302, Anton Paar, Austria) to simulate the shear conditions that occur during pile penetration. All samples were tested within approximately 1 min after Cr^{3+} addition to the XG solution to capture their early-stage rheological response before substantial gelation occurred.

Two types of tests were performed to evaluate the rheological properties of the XG and Cr–XG hydrogels under various conditions. First, rotational tests were conducted over a shear-rate range of 0.01–1000 s^{-1} to assess the shear-thinning properties of the hydrogels. The apparent viscosity was measured at various shear rates. This explains the shear rate-dependent behavior of the XG and Cr–XG hydrogels.

Second, oscillatory shear tests were performed over a shear-strain range of 0.01%–1000% to determine the yield stress and flow point of the hydrogels. In the resulting storage modulus (G')–shear-strain curves, the linear viscoelastic region ends at a certain shear stress level, which is defined as the yield stress. The flow point is defined as the shear stress at which the storage (G') and loss (G'') moduli intersect.

By comprehensively analyzing the rotational and oscillatory test results, the shear-thinning behavior with increasing shear rate, initial yield stress, and flow-transition points can be quantified. These parameters are directly relevant for understanding lubrication effects during pile penetration and adhesion development after curing, thereby linking lab-scale rheological behavior to the mechanical interpretation of pile performance. These rheological parameters reflect the pre-gelation behavior of the hydrogels, which may differ from their fully crosslinked state; this limitation should be noted when interpreting the results.

2.4 Direct and interface shear tests

Direct shear tests were conducted to evaluate the shear strength parameters of the Cr–XG-treated soils. Laboratory-scale direct shear tests were performed according to ASTM D3080 (ASTM 2011), with soil samples with an outer diameter of 60 mm and a height of 20 mm placed in the shear box. Vertical stresses of 50, 100, and 200 kPa were applied to the soil, and the shear rate was set to 1.0 mm/min. Displacement transducers were used to measure the shear and vertical displacements during shearing, and a load transducer was used to measure the shear stress corresponding to the developed shear strain. Each laboratory test was performed three times per vertical stress to ensure repeatability. Using each vertical stress and its corresponding peak shear strength, the Mohr–Coulomb failure envelope was plotted to determine the cohesion and friction angles of the soil samples and expressed using the mean and standard deviation of all data for each load. For the shear stress-shear strain and vertical strain-shear strain relationships, representative curves are presented, which correspond to the test results yielding peak strengths closest to the averaged values used for the Mohr-Coulomb failure envelope. The apparatus used for the direct shear tests is shown in Fig. 2(a).

The interface friction and adhesion between the pile surface and soil affect the bearing capacity and pullout resistance of the pile. Interface shear tests were conducted to evaluate the effect of the Cr–XG hydrogel on the interface shear behavior and strength development between the pile and soil particles. The same shearing device used in the direct shear tests was employed for the interface shear tests with vertical stresses of 50, 100, and 200 kPa. An acrylic plate with a diameter of 60 mm and height of 10 mm was placed at the bottom of the shear box to simulate frictional condition between the soil and pile. Additionally, #120 sandpaper was attached to the top of the acrylic plate to simulate the surface-friction conditions of the steel pile. This can help exclude the influence of soil particle effects on interface behavior and enable the universal application of research results. The pile model used in this study was made of PVC pipe, and acrylic plates were used in interface shear tests. Compared to field piles constructed with steel pipes or concrete, PVC pipe has lower interface shear resistance. Using PVC pipe directly in model tests could underestimate the actual penetration resistance and pullout resistance. Therefore, #120 sandpaper was applied to reflect

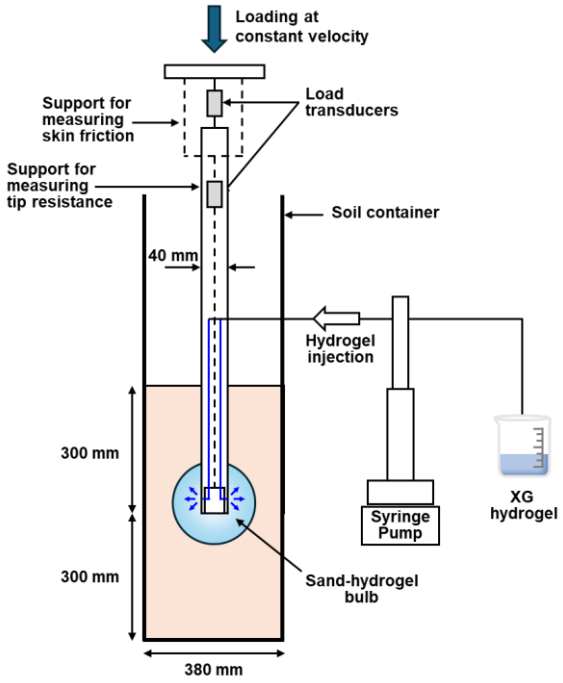

Fig. 3 Systematic diagram of pile penetration tests

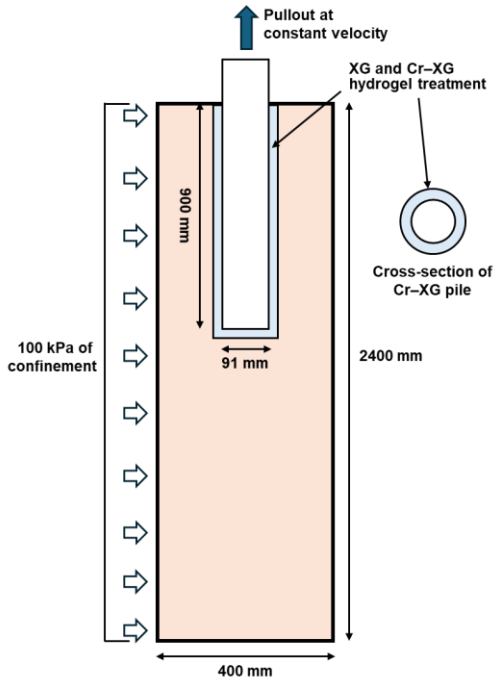

Fig. 4 Systematic diagram of pile pullout tests

the skin friction commonly occurring on field piles. Preliminary experiments confirmed that the interface behavior between the #120 sandpaper and the soil exhibits friction similar to soil-soil interaction (friction angle), validating the feasibility of the sandpaper. The maximum surface roughness (R_t) of the sandpaper was 0.169 μm, and the normalized surface roughness (R_n) was 0.12. The same procedures and apparatus used in the direct shear tests were employed to measure the shear stress, shear displacement, and vertical displacement of the soils. The apparatus used for the interface shear tests is shown in Fig. 2(b).

2.5 Penetration tests on piles with Cr–XG hydrogels

Laboratory-scale pile-penetration tests were conducted to assess the effect of the XG hydrogel on pile penetration (Fig. 3). The soil chamber, which was made of transparent acrylic, had a diameter of 380 mm and height of 950 mm. The pile model, which was made of polyvinyl chloride, had a diameter of 40 mm and height of 740 mm. As shown in Fig. 3, the loading and measurement system used in the pile-penetration tests could simultaneously measure the end bearing generated at the pile tip and skin friction generated at the pile side without interference. Furthermore, the bearing capacity of the pile during penetration was determined using the total load, which was the sum of the measured end bearing and skin friction. The surface of the pile model was covered with #120 sandpaper to simulate the surface of a steel pile. The model ground was prepared using a sand pluviator from a constant height of 50 cm to achieve a dry unit weight of 16.3 kN/m³. The tip of the pile was positioned 30 cm above the bottom of the soil chamber. To evaluate whether the XG and Cr–XG hydrogels reduce the pile-penetration resistance, it was injected simultaneously with pile penetration. Three injection ports were installed in the pile-tip section, and a high-pressure injection pump (syringe pump, ISCO 500D, Teledyne, USA) was used for hydrogel injections. During penetration, the XG hydrogel was injected at a constant pressure of 100 kPa. XG hydrogels at concentrations of 2.5% and 5.0% m_x/m_w were used, and the Cr/XG ratio was set to 30% for Cr–XG. The penetration of the pile model was performed at a speed of 1 mm/min, and the pile model was driven to a maximum penetration depth of 40 mm.

2.6 Pullout tests on piles with Cr–XG hydrogels

After all pile installations are completed, an in-situ pullout test is performed to evaluate whether the installation was successful. In this study, model pullout tests were conducted by assuming that the pile was driven to a sufficient embedded depth with the XG/Cr–XG hydrogel. The pullout-test apparatus is illustrated in Fig. 4. The soil chamber had a length of 2400 mm and width and height of 400 mm each. The pile model had a diameter of 91 mm and length of 900 mm. Sandpaper identical to that used in the penetration tests was attached to the pile model used in the pullout tests. The side walls of the soil chamber were configured to accommodate displacement and loading. A confinement pressure of 100 kPa was applied to the side walls to simulate in-situ soil conditions. The model ground was prepared using a sand pluviator. Sand was spread from a constant height of 60 cm to create a model ground with a dry unit weight of 16.3 kN/m³. To evaluate the effect of the XG and Cr–XG hydrogels on pullout resistance, 0.5% and 1.0% of m_x/m_s was applied. Specifically, the Cr/XG ratio was set to 30% for Cr–XG. For the XG and Cr–XG treatments, the soil and hydrogel were mixed and applied to a pile surface with a thickness of 4 mm. After installing the ground and pile models, a confining pressure of 100 kPa

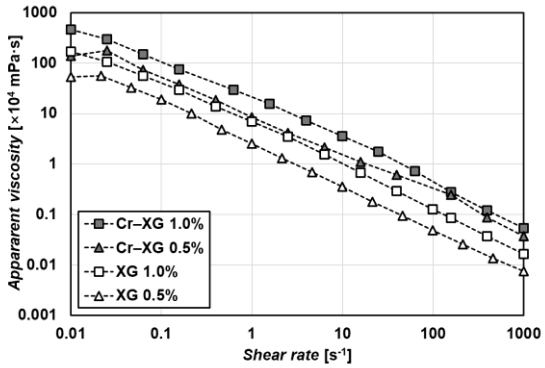

Fig. 5 Variation of apparent viscosity for each hydrogel

was applied to the side walls of the soil chamber to simulate the in-situ ground conditions. The pile model was pulled out at a rate of 1 mm/min and the pullout displacement was recorded up to a maximum of 30 mm. The pullout resistance and displacement were recorded in real time.

3. Test results and discussion

3.1 Rheological properties of Cr–XG hydrogels

3.1.1 Rotational tests: shear-thinning behavior

Rotational tests were performed to analyze the apparent viscosity behavior of XG and Cr–XG hydrogels when subjected to a shear rate, as shown in Fig. 5. All hydrogels exhibited shear-thinning behavior, where the apparent viscosity decreased as the shear rate increased. For the XG hydrogels, a higher apparent viscosity was observed at higher concentrations, which can be attributed to increased polymer-chain entanglement and hydrogen bonding (Zhong *et al.* 2013, Kummar *et al.* 2025). Furthermore, the additional increase in the apparent viscosity of Cr–XG is attributed to the initial strengthening of the gel network owing to Cr^{3+}-carboxylate coordination crosslinking (Hansen and Lund 1995, Shibaev *et al.* 2020). The shear-thinning behavior, in which the apparent viscosity decreases sharply with increasing shear rate, is expected to have a lubricating effect in high-shear areas at the pile tip and skin during penetration. Conversely, in the low-shear state (during the static and curing phases), a higher viscosity is considered advantageous for interface bonding and the formation of soil-pile adhesive components.

3.1.2 Oscillatory tests: yield stress and flow point

The phase-transition range and yield stress of the XG and Cr–XG hydrogels under oscillatory shear strain were determined via oscillatory experiments using a rheometer (Fig. 6). For all the hydrogels, both the storage and loss moduli remained constant without decreasing up to a shear strain of 0.01%–10%. The shear stress at this point is defined as the yield stress. Conversely, when the shear strain exceeded 10%, the storage and loss moduli intersected; this point is defined as the flow point. An increase in the XG concentration and the addition of Cr^{3+} ions induced increases in both yield stresses and flow

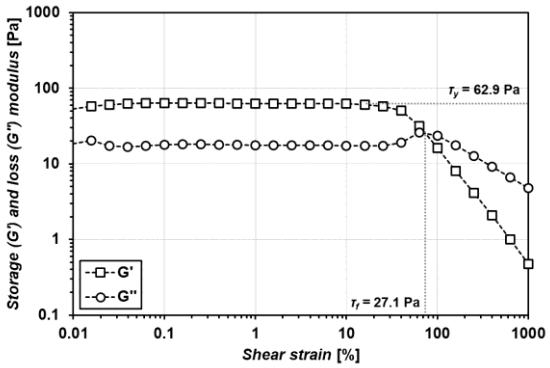

(a) XG 0.5%

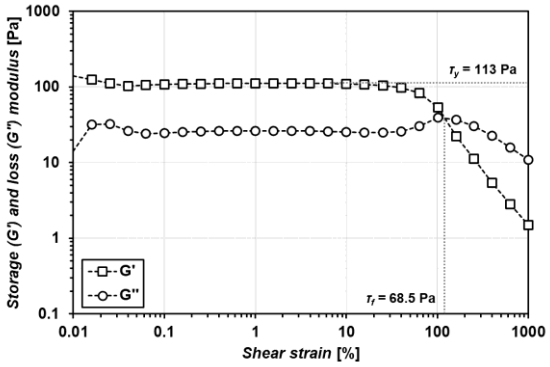

(b) XG 1.0%

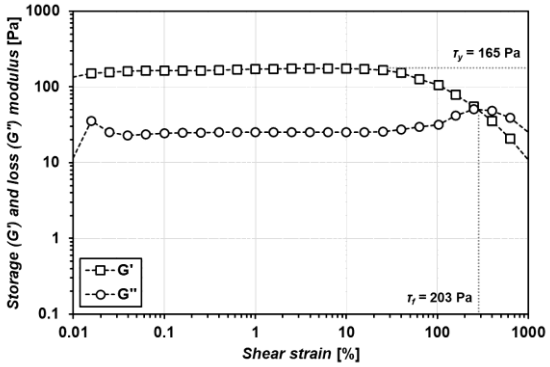

(c) Cr–XG 0.5%

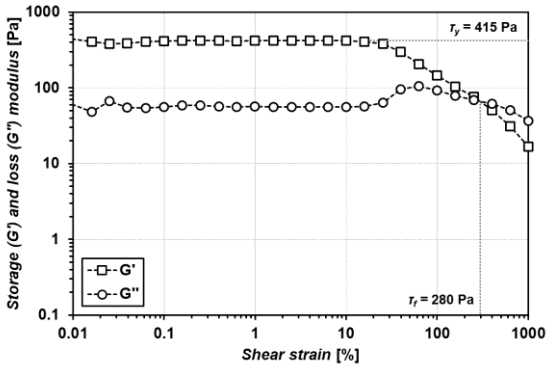

(d) Cr–XG 1.0%

Fig. 6 Oscillatory test results for each hydrogel

points. Higher yield stresses and flow points suggest improved pile stability, structural retention at low shear strains, and enhanced interface adhesion, exhibiting a trend similar to that of the variation in apparent viscosity. This is

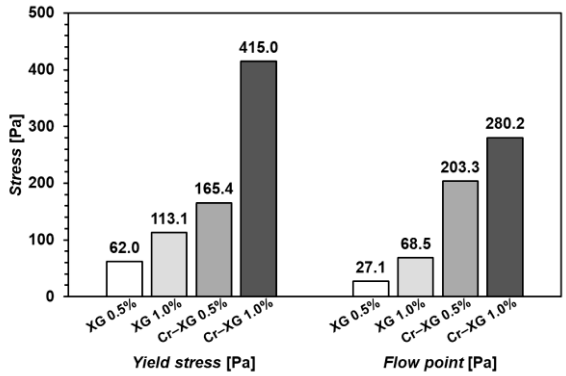

Fig. 7 Yield stresses and flow points for each hydrogel

related to the post-construction performance of the pile–soil system. In contrast, rotational tests primarily identify the viscosity reduction under high-shear conditions related to penetration resistance during construction. These two tests provide complementary insights. Rotational tests evaluate lubrication effects during pile driving, whereas oscillatory tests assess post-curing adhesion. The determined yield stresses and flow points are shown in Fig. 7.

3.2 Shear strength properties of Jumunjin sand

Direct shear tests were performed to determine the shear strength characteristics of Jumunjin sand and evaluate the shear strength enhancement of XG/Cr–XG soils. Fig. 8 shows the shear stress and vertical strain as the vertical stress was increased to 50, 100, and 200 kPa. For the shear stress–strain curves (Fig. 8(a)), the soil subjected to 50 kPa of vertical stress exhibited the lowest peak shear strength (33.7 kPa), whereas the soil under 200 kPa of vertical stress showed the highest peak shear strength of 134.9 kPa. For the vertical strain–shear strain relationships (Fig. 8(b)), the soil subjected to 50 kPa of vertical stress exhibited the highest dilation, whereas the soil under 200 kPa of vertical stress showed the lowest dilation. This is because a higher vertical stress restrains the dilation and expansion induced by shear strain. The shear strength parameters of the soil were determined using the vertical stress and corresponding peak shear stress (Fig. 8(c)). Based on direct shear tests, the shear strength parameters (cohesion and friction angle) of the Jumunjin sand were determined to be 0 kPa and 34°, respectively.

3.3 Shear strength properties of XG- and Cr–XG-treated soils

For the XG-treated soils (Figs. 9(a) and 9(b)), the shear stress gradually increased with increasing shear strain, reached a peak, and then failed, followed by a slow decrease in stress. Furthermore, XG-treated soils exhibited a higher peak shear stress in soils with m_x/m_s = 1.0% compared to those with m_x/m_s = 0.5%, suggesting that m_x/m_s influences soil strength. In contrast, Cr–XG-treated soils showed a steeper initial increase in shear stress than XG-treated soils and reached higher peak shear stresses (Figs. 9(c) and 9(d)). Furthermore, Cr–XG-treated soils with

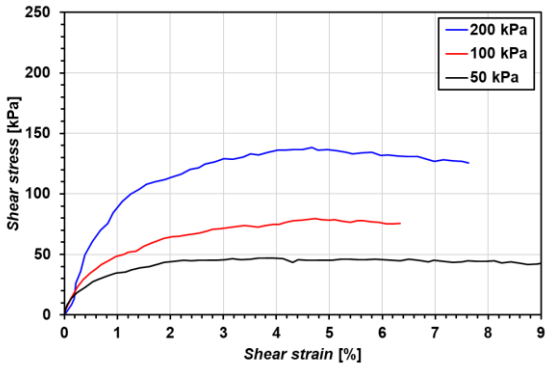

(a) Shear stress–shear strain

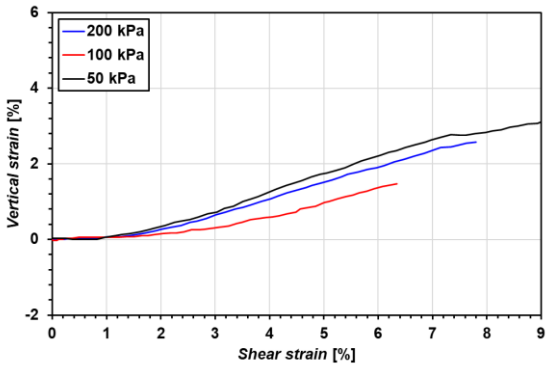

(b) Vertical strain–shear strain

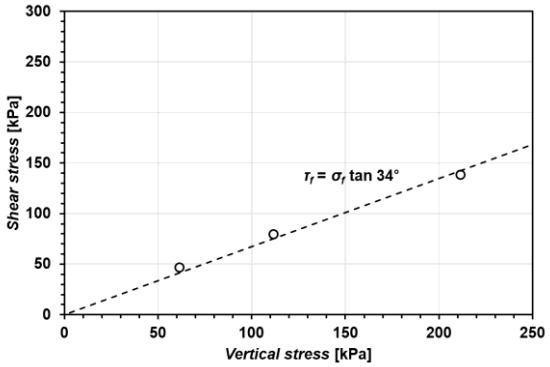

(c) Mohr–Columb failure envelope

Fig. 8 Direct shear test results of Jumunjin sand

m_x/m_s = 0.5% exhibited a higher shear strength than soil with m_x/m_s = 1% and without Cr^{3+} ion addition. This suggests that combining Cr^{3+} with XG enables a higher shear strength that can be achieved even at lower m_x/m_s concentrations. Furthermore, for the Cr–XG-treated soils, a rapid decrease in strength was observed after the peak shear stress was reached, indicating that Cr–XG-treated soils exhibited more brittle behavior than XG-treated soils

For the vertical- and shear-strain relationships (Figs. 9(e)-9(h)), all treated soils initially exhibited compressive behavior, followed by expansive behavior as the shear strain increased, unlike the control condition. The relative density of the control soil was 57%, with a corresponding void ratio of 0.63. Sandy soils under these conditions exhibit no dilative behavior following contractive behavior, only weak preferred orientation (Mitchell and Soga 2005), which is consistent with the behavior observed in this study (Fig. 8(b)). In contrast, treated soils developed high friction angle

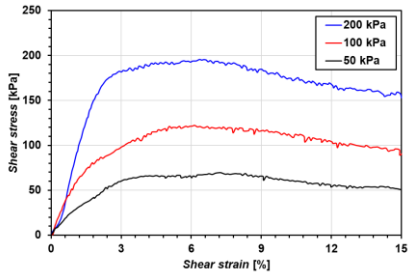

(a) Shear stress–strain of XG 0.5%

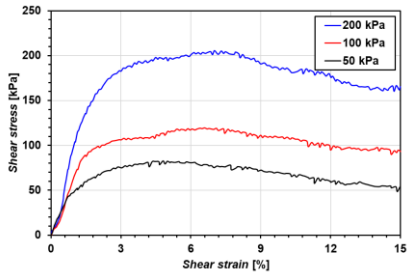

(b) Shear stress–strain of XG 1.0%

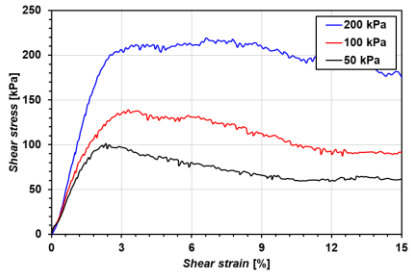

(c) Shear stress–strain of Cr–XG 0.5%

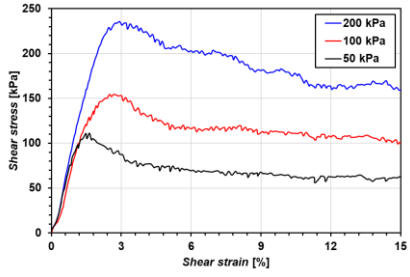

(d) Shear stress–strain of Cr–XG 1.0%

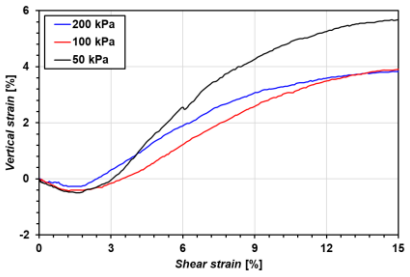

(e) Vertical- and shear-strain c XG 0.5%

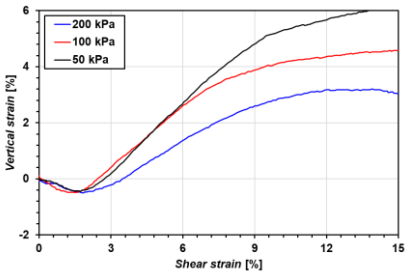

(f) Vertical- and shear-strain of XG 1.0%

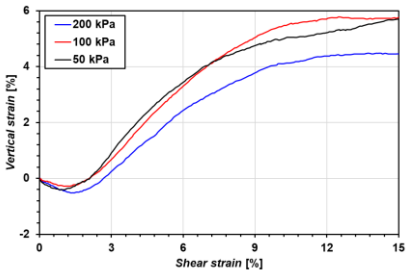

(g) Vertical- and shear-strain of Cr–XG 0.5%

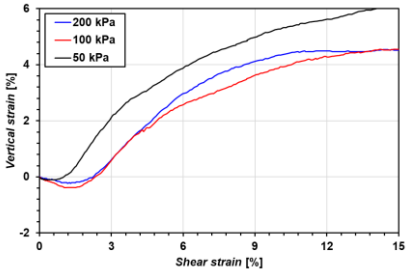

(h) Vertical- and shear-strain of Cr–XG 1.0%

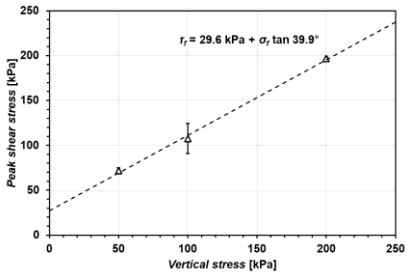

(i) Mohr–Coulomb failure envelope of XG 0.5%

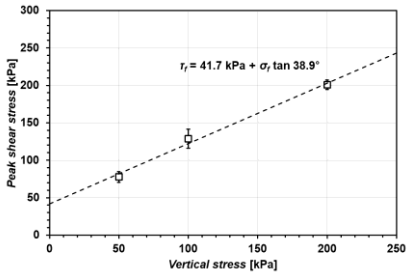

(j) Mohr–Coulomb failure envelope of XG 1.0%

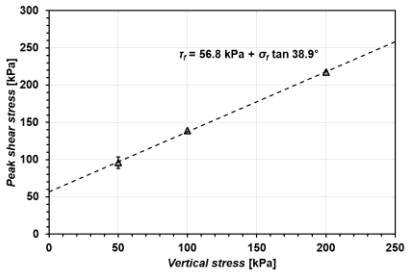

(k) Mohr–Coulomb failure envelope of Cr–XG 0.5%

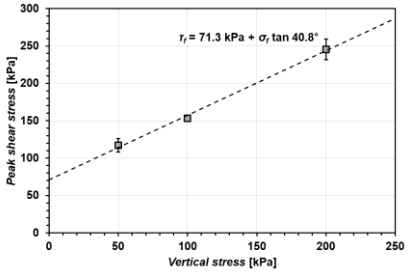

(l) Mohr–Coulomb failure envelope of Cr–XG 1.0%

Fig. 9 Direct shear test results of XG- and Cr–XG-treated soils

Table 1 Shear strength parameters of XG- and Cr–XG-treated soils

Test variables	Cohesion [kPa]	Friction angle [°]
Sand	0	34.0
XG 0.5%	29.6	39.9
XG 1.0%	41.7	38.9
Cr–XG 0.5%	56.8	38.9
Cr–XG 1.0%	71.3	40.8

and cohesion due to interparticle bonding, leading to dilative behavior (Bang *et al.* 2025). Furthermore, this behavior is typically observed in dense soils, suggesting that both the XG and Cr–XG treatments promote the development of a structural skeleton in dense soils. This trend aligns with previous literature, indicating that Cr–XG prevent particle deformation through mechanical bonding (Bang *et al.* 2025).

The shear strength of the treated soils was characterized using the Mohr–Coulomb failure envelope (Figs. 9(i)-9(l)). A small increase in the friction angle of treated soils was observed with XG concentration or Cr^{3+} addition. Conversely, cohesion increased with higher XG concentrations, and at the same XG concentration, the addition of Cr^{3+} further enhanced cohesion. This behavior is attributed to the time-dependent dehydration of XG and the

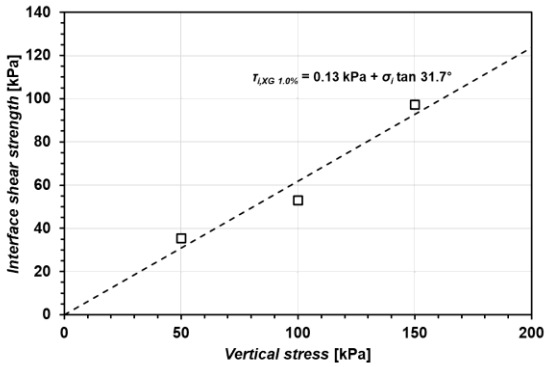

(a) XG 0.5%

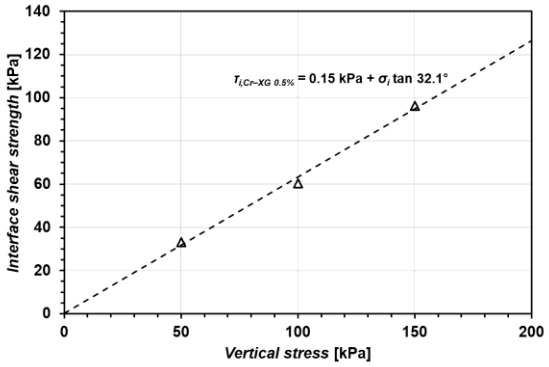

(b) XG 1.0%

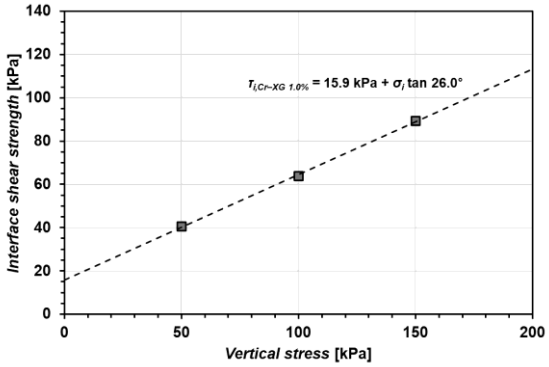

(c) Cr–XG 0.5%

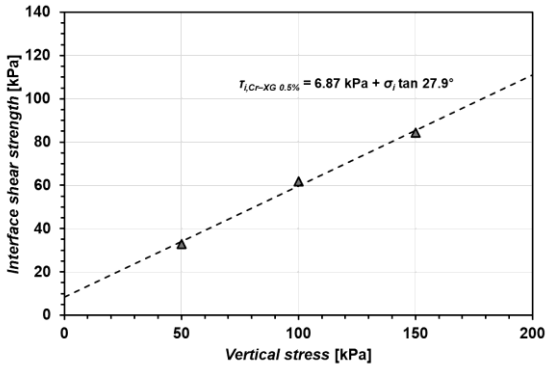

(d) Cr–XG 1.0%

Fig. 10 Interface shear behavior of XG- and Cr–XG-treated soils

pore-filling rigidity of Cr–XG (Lee *et al.* 2023b, Bang *et al.* 2025), which enhance interparticle bonding and restrain particle deformation. This suggests that while XG and Cr–XG do not affect interparticle friction behavior, cohesion in soils can be significantly improved by increasing the XG concentration or through Cr^{3+} crosslinking. The shear strength parameters determined from the direct shear tests are listed in Table 1.

Table 2 Interface shear strength parameters of XG- and Cr–XG-treated soils

Test variables	Interface adhesion [kPa]	Interface friction angle [°]
Sand	0	32.3
XG 0.5%	0.15	32.1
XG 1.0%	0.13	31.7
Cr–XG 0.5%	6.87	27.9
Cr–XG 1.0%	15.9	26.0

3.4 Interface shearing behavior of XG and Cr–XG soils

The shear behavior at the pile–soil interface was assessed through interface shear tests. Unlike direct shear tests that determine the soil friction angle and cohesion, interface shear tests determine the interface adhesion and friction angle. This section compares the interface shear behavior under the pile–soil, pile–XG, and pile–Cr–XG conditions. The interface shear behavior and determined shear parameters are shown in Fig. 10 and Table 2, respectively.

Adhesion did not occur at the pile–soil interface, and the friction angle was nearly identical to that of the untreated sand, indicating that pure friction behavior dominated. For the XG-treated soils (m_x/m_s = 0.5% and 1.0%), only slight adhesion occurred, and the interface friction angle decreased further compared to the control (Figs. 10(a) and 10(b)). This is attributed to the lubricating effect of the hydrated hydrogel at the XG–sandpaper interface. Cr–XG-treated soils exhibited a smaller interface friction angle than the control and XG-treated samples, but showed higher interface adhesion than the other soils (Fig. 10c and d). This is owing to the enhanced network formation and bridging between the Cr–XG hydrogel and sandpaper. This suggests that the XG and Cr–XG treatments do not affect the interparticle friction behavior but significantly influence interface adhesion, which is consistent with the results derived from the direct shear tests.

3.5 Effect of Cr–XG hydrogels on initial penetration resistances of piles

The effect of the XG-hydrogel injection on the initial penetration resistance of the pile models was investigated through laboratory-scale penetration tests. The penetration tests considered five test conditions: (i) untreated (Control) piles in sandy ground and piles with (ii) 0.5% XG hydrogel (XG 0.5%), (iii) 1.0% XG hydrogel (XG 1.0%), (iv) 0.5% crosslinked XG hydrogel (Cr–XG 0.5%), and (v) 1.0% crosslinked XG hydrogel (Cr–XG 1.0%). The pile-model configuration allowed separate measurements of the end bearing and skin friction, as shown in Fig. 3. The penetration results of the piles are shown in Fig. 11.

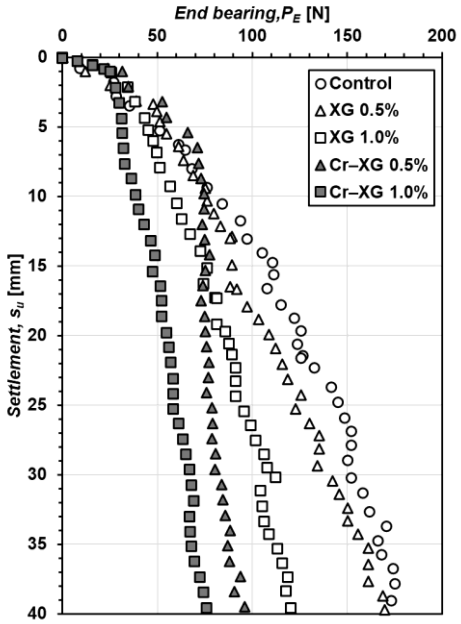

(a) End bearing

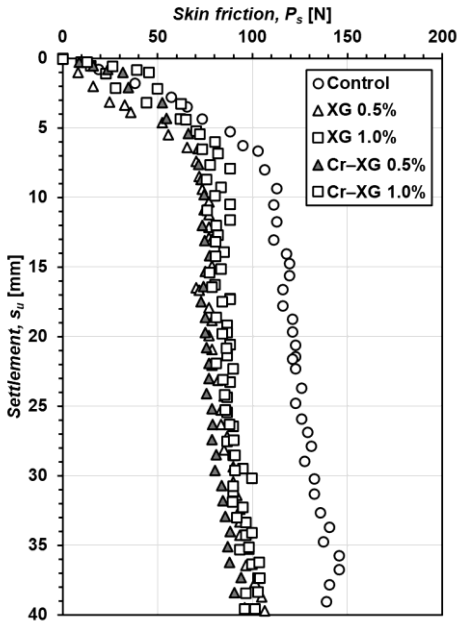

(b) Skin friction

Fig. 11 Penetration resistances of piles

In all cases, the end bearing increased without a peak as the penetration depth increased (Fig. 11(a)). During the final settlement stage, the reduction in the end bearing resulted in a smaller end bearing (169.7 N) in the XG 0.5% case compared to the control (179.5 N); however, the reduction effect was not significant at 5.46%. When the XG 1.0% hydrogel was injected, the final end bearing was 120.2 N, exhibiting a decrease of approximately 33.04% compared with the control. Furthermore, the end bearings determined for crosslinked XG cases (Cr–XG 0.5% and 1.0%) were 94.1 N and 75.3 N, showing reduction rates of 47.58% and 58.05%, respectively. This reduction in the end bearing was owing to the shear-thinning behavior, where the viscosities of the XG and Cr–XG hydrogels decreased with increasing shear strain. During pile penetration, the injected hydrogel layer near the pile tip encountered high shear strain, reducing its viscosity. Rheological test results (Figs. 5 and 6) showed that increasing the XG concentration and Cr^{3+} ions increased both yield stresses and flow points under stress. During pile penetration, the injected hydrogel layer near the pile tip underwent high shear strain, reducing its viscosity. Solutions with low flow points (XG 0.5% and 1.0%) exhibited liquid behavior under high shear strain, losing their viscoelastic properties. Conversely, solutions with high flow points and yield stresses maintained their viscoelastic characteristics when subjected to high shear strains. The viscoelastic properties of the solution directly reduced the penetration resistance of the pile; therefore, the pile with Cr–XG 1.0%, which had the highest yield stress and flow point among all cases, exhibited the highest reduction ratio in penetration resistance. This resulted in a lower end bearing, facilitating easier pile penetration.

In contrast, skin friction exhibited the same reduction effect for all cases (XG 0.5% and 1.0%, Cr–XG 0.5% and 1.0%) compared with the control (Fig. 11(b)). This suggests that the thin hydrogel layer along the pile shaft acted as a lubricating interface (Stokes *et al.* 2011), enabling skin friction reduction regardless of the XG concentration. Thus, unlike the end bearing, where the hydrogel viscosity dominates the response, skin friction appears to be controlled by the presence of the lubricating film rather than the rheological strength.

The total load applied to the pile was calculated by adding the end bearing and skin friction loads, and the ultimate bearing capacities of the pile were derived from the load-settlement curves. Several methods may be used to determine the ultimate bearing capacity of a pile from a load-settlement curve (Vesić 1963, Housel 1966, Hirany and Kulhawy 1988). The Davisson offset method (Davisson 1972), which is widely used, was applied in this study. This method involves drawing an extension line of the initial linear portion of the load-settlement curve. The ultimate bearing capacity is then determined as the point at which this final line intersects the load-settlement curve after being offset axially by (0.15 in + D/120). The total load-settlement curves and ultimate bearing capacities are shown in Fig. 12. The highest ultimate bearing capacity of 206.5 N was determined for the control (Fig. 12(a)). The ultimate bearing capacities of the piles with XG 0.5% and 1.0% were determined to be 160.0 N and 131.3 N, respectively (Figs. 12(b) and 12(c)). Lower ultimate bearing capacities were determined compared to other variables for the XG cases with added Cr^{3+} (Figs. 12(d) and 12(e)). The ultimate bearing capacities of the Cr–XG 0.5% and 1.0% piles were determined to be 120.7 N and 103.6 N, respectively. Compared with the control, the injection of XG hydrogel and pile penetration resulted in lower ultimate bearing capacities. Notably, the reduction in the ultimate bearing capacity was more effective when Cr^{3+} was added. These results demonstrate that in-situ hydrogel injection during pile installation can effectively reduce end bearing and skin friction, and the penetration resistance effect was the most significant in the Cr–XG 1.0% case. Regardless of the

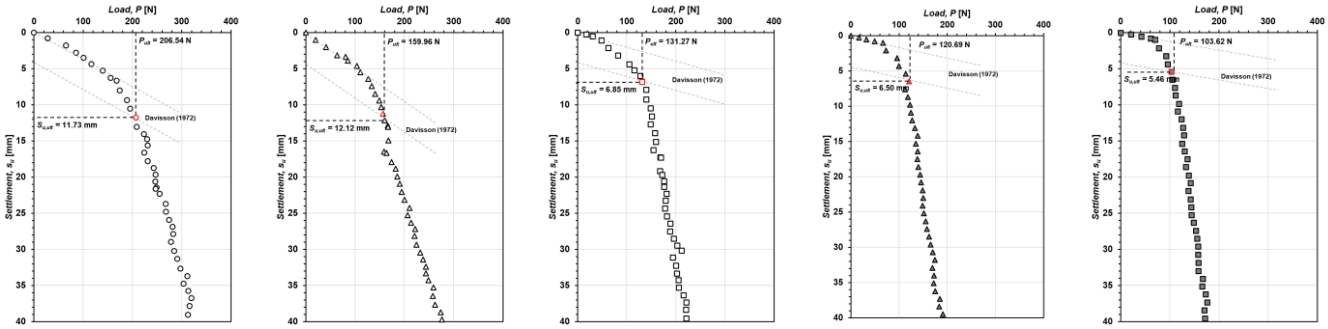

(a) Control (b) XG 0.5% (c) XG 1.0% (d) Cr–XG 0.5% (e) Cr–XG 1.0%

Fig. 12 Total load-settlement curves and ultimate bearing capacities of piles

concentration, the decrease in skin friction, even with a minimal injection of the XG hydrogel, suggests the field applicability of energy-efficient piles.

3.6 Effect of Cr–XG hydrogels on pullout resistance of piles

Following the penetration-test procedure, the installation was considered complete when the desired penetration depth of the pile was reached. Unlike the penetration test, pullout tests were performed to evaluate the effect of the Cr–XG-hydrogel injection on the pullout resistance after pile installation. The variables for the pullout tests were identical to those used in the pile-penetration tests. The failure load determined by the pullout tests was measured using the Davisson offset method, which was the same method used to determine the ultimate bearing capacity of the pile. The pullout-test results for each case are shown in Fig. 13.

The failure load of the pile owing to pullout was determined to be 9.74 kN for piles in sandy ground (Fig. 13(a)). The failure loads of the piles with only XG 0.5% and 1.0% hydrogel applied to their surfaces were 5.92 kN and 7.86 kN, showing 39.2% and 19.3% reductions in pullout resistance compared to the control, respectively (Figs. 13(b) and 13(c)). This was owing to the shear behavior at the hydrogel-pile interface. As shown in Fig. 10, the XG-treated soils exhibited a slightly lower interface friction angle and slightly higher interface adhesion than the control. Consequently, when only XG was applied, the shear resistance generated at the interface was relatively low, resulting in a lower pullout resistance. Furthermore, when using only XG for pile installation, the penetration resistance decreased; however, the subsequent pullout resistance also decreased, resulting in an insufficient load-bearing capacity. For the pile treated with Cr–XG 0.5%, a failure load of 9.14 kN was determined, which exhibited a significantly lower reduction rate (6.16%) than that of the XG treatment. Conversely, for the Cr–XG-treated piles (Fig. 13(e)), a 6.47% higher failure load was confirmed compared with the control. This was owing to the high interface adhesion generated between the Cr–XG soils and pile interface. From an in-situ application perspective, a two-stage strategy was confirmed to be effective: during installation, the shear-thinning lubrication effect of Cr–XG reduced penetration resistance, and after installation, Cr^{3+} cross-linking increased pullout resistance. Specifically, the use of the Cr–XG hydrogel instead of XG at a concentration of 1.0% increased the pullout resistance. This approach enabled the simultaneous improvement in construction performance through a low penetration resistance and structural performance through a high pullout resistance.

Furthermore, when piles were pulled out, their pullout resistances exhibited higher fluctuations compared to the control. As shown in Fig. 13(a), the control pile maintained its pullout resistance within a certain range even after reaching the failure load. In contrast, as shown in Figs. 13(b)-13(e), the XG- and Cr–XG-treated piles were not able to maintain a constant pullout resistance after the failure load and exhibited fluctuations. This is attributed to the differences in the characteristics of the hydrogels. In the case of XG, when the XG hydrogel dehydrates, it exhibits higher brittleness behavior compared to its hydrated state (Kumar and Sujatha 2021, Weng *et al.* 2021, Jiang *et al.* 2022). This brittleness affected the fluctuations observed after the failure load. This trend is consistent with the direct shear test results (Figs. 9(a) and 9(b)) in this study. Conversely, for Cr–XG hydrogels, the fluctuation is attributed to their phase transition characteristics based on curing time. Cr–XG hydrogel transitions from viscoelastic property to elastic behavior over time, indicating hydrogel behavior as a solid (Lee *et al.* 2023a). Furthermore, Cr–XG hydrogels exhibit irreversibility, meaning their cohesive structure does not recover after failure (Marudova-Zsivanovits *et al.* 2007). Due to this characteristic, while the pile can maintain a constant pullout resistance beyond the failure load (Park *et al.* 2024b), its fluctuations were shown to be similar to those of XG hydrogels, with the magnitude of these fluctuations analyzed to be greater than that of XG.

3.7 In-situ application strategy for installing bioinspired piles

The laboratory test results revealed two key mechanisms related to field applications. During pile penetration, the XG and Cr–XG hydrogels exhibited significant shear-thinning behaviors under high-shear-rate conditions, effectively reducing the end bearing and shaft friction. After penetration completion, Cr^{3+} crosslinking formed an interface network, increasing adhesion and pullout resistance. These results provide a basis for an in-situ

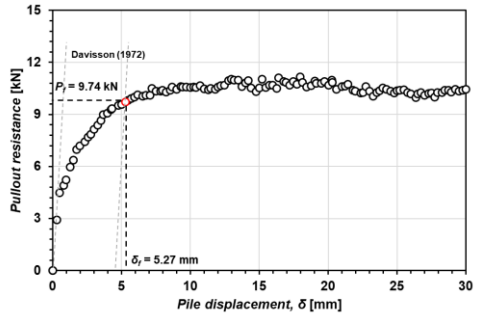

(a) Control

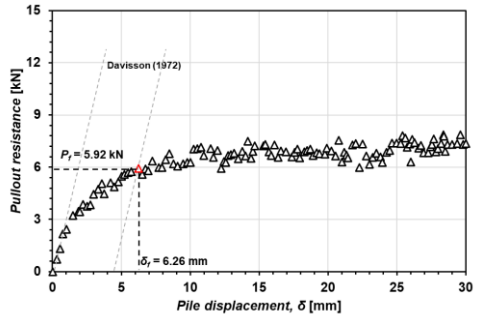

(b) XG 0.5%

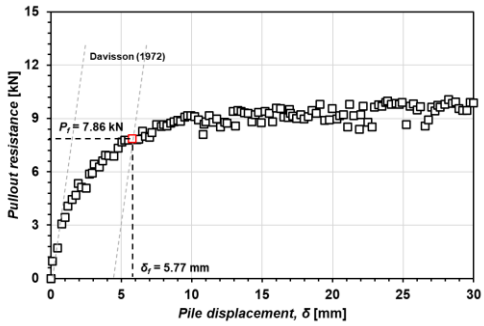

(c) XG 1.0%

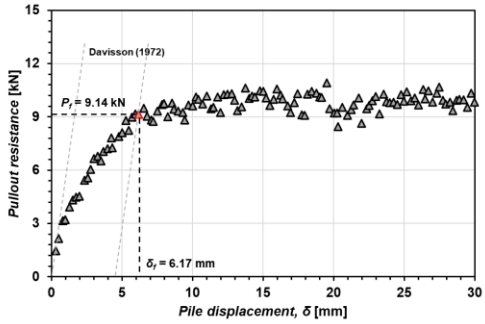

(d) Cr–XG 0.5%

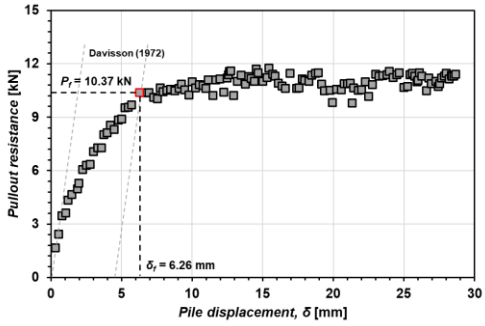

(e) Cr–XG 1.0%

Fig. 13 Pullout resistances and failure loads of piles

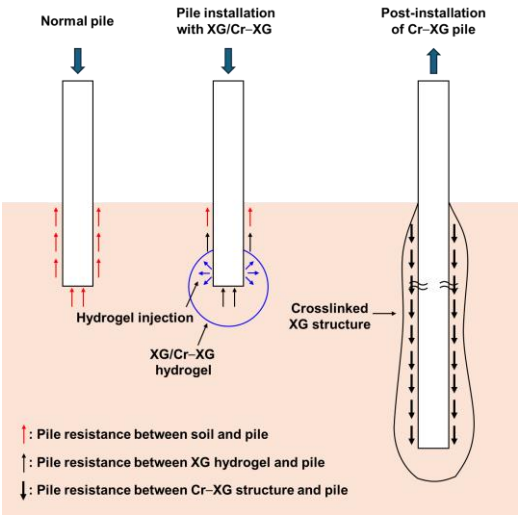

Fig. 14 Mechanism for improving the efficiency of pile penetration and pullout resistance with XG and Cr–XG

installation strategy that utilizes a low apparent viscosity under high-shear-strain conditions to enhance the penetration efficiency and secure high interface-bonding strength through controlled gelation after construction. During pile driving, the injected hydrogel plausibly forms a thin annular film along the pile surface, reducing the interface shear rate and thus the initial skin friction; after installation, progressive gelation and interparticle bonding restore adhesion and secure long-term stability at the pile–soil interface. This section presents strategies and methods for in-situ applications by integrating the laboratory test results. The proposed mechanism of the bioinspired pile is shown in Fig. 14.

The common construction methods used in field applications include impact driving, vibratory driving, and bored cast-in-place piling. Among these, impact and vibratory driving are particularly suitable for installing bioinspired piles because they enable simultaneous hydrogel injection during the driving process, making them directly compatible with the method proposed in this study. In the proposed system, a tip-injection system near the pile tip ensures a continuous hydrogel supply during penetration. During pile driving, the hydrogel maintained a shear-thinning state, reducing the pile penetration resistance.

Upon reaching the target depth and stopping penetration, Cr^{3+}–XG coordination proceeded, naturally forming a pile–soil interface bond within a specific curing period.

In particular, for vibratory driving, cyclic shear is expected to further enhance the shear-thinning effect, enabling continuous lubrication and minimal ground disturbances during penetration (Park *et al.* 2025). Conversely, synchronizing the impact energy with the hydrogel-injection timing can achieve a similar effect during impact driving. Both methods provide effective approaches for the in-situ application of Cr–XG bioinspired piles, demonstrating the potential to simultaneously ensure construction efficiency and post-construction structural stability.

3.8 Limitations and further studies

This study is a laboratory-scale investigation using Jumunjin sand; thus, it cannot directly represent pile behavior under actual fine-grained soil, saturated soil, and composite ground conditions. Furthermore, the use of a high-pressure syringe pump does not consider field variables that may be encountered during actual construction, such as in-line mixing residence time, nozzle clogging, and injection pressure fluctuations.

The penetration and pullout tests in this study were performed under constant-rate loading conditions, whereas actual field installation often involves dynamic methods such as pile driving or vibratory penetration. This discrepancy may affect the mobilized soil–pile interaction and should be recognized as a limitation of the present investigation.

In the pullout tests of the piles, the ratio of the soil chamber diameter to the pile diameter was approximately 4.4, which is below the threshold of 7 to 20 where boundary effects typically do not occur (Dong *et al.* 2018, Gamez and Olson 2022, Park *et al.* 2024a). Therefore, since boundary effects could potentially have occurred, changes in confining pressure during pile displacement were measured in real time to indirectly evaluate the boundary effect. Measurement results showed no pressure changes observed at the side walls, suggesting the boundary effect was likely limited. However, this approach alone has limitations in quantitatively determining the presence and extent of the boundary effect. Therefore, subsequent research should verify and supplement the influence of the boundary effect through numerical modeling based on the same experimental conditions.

Finally, for the pullout test, it was performed assuming the hydrogel was uniformly distributed on the pile surface. However, under actual in-situ conditions, the hydrogel may be distributed irregularly on the pile surface. Since this could lead to discrepancies between laboratory test results and actual construction results, further research is necessary to analyze the actual distribution pattern of the hydrogel through bench-scale tests.

Further research is suggested to verify the applicability of the proposed hydrogels through field pilot tests and large-scale 1-G simulation experiments and numerical simulations, the evaluation of long-term durability considering wetting–drying/freezing–thawing conditions, and the assessment of sustainability via Cr^{3+} environmental impact and life cycle assessment. In addition, further investigation should include quantification of the Cr^{3+}:carboxylate molar ratio, pH variation during gelation, and the gelation-time window to better elucidate the crosslinking mechanism of the Cr–XG hydrogels.

4. Conclusions

The present study has experimentally validated the concept and feasibility of a bioinspired pile system utilizing a Cr–XG hydrogel. The hydrogel exhibited shear-thinning behavior, characterized by a decrease in apparent viscosity with increasing shear rate. Additionally, it demonstrated enhanced initial viscosity and yield stress at higher XG concentrations and with Cr^{3+} crosslinking. Furthermore, oscillatory shear tests showed an increase in flow point, implying improved structural stability and interfacial adhesion under static conditions. The rheological characteristics of the hydrogel support its dual functionality: facilitating penetration during installation and promoting mechanical bonding afterwards.

Shear strength tests confirmed that both XG concentration and Cr^{3+} addition contributed to increased cohesion and friction angle, especially under the XG 1.0%–Cr^{3+} condition. This observation was consistent in interface shear tests, thereby reinforcing the improvement in pile-soil interfacial behavior. In penetration tests, hydrogel-treated piles exhibited reductions in both end bearing and skin friction, more notably with higher XG concentration, resulting in a decrease in ultimate bearing capacity—but with enhanced installation efficiency. Conversely, the Cr–XG-treated piles provided the highest pullout resistance, suggesting the potential to achieve a balance between reduced penetration resistance during installation and ensuring post-installation structural stability.

Acknowledgments

This work was supported by the National Research Foundation of Korea (NRF) grant funded by the Korea government (MSIT) (No. 2022R1A2C2091517).

References

Ahmad, N.H., Mustafa, S. and Che Man, Y.B. (2015), "Microbial polysaccharides and their modification approaches: A review", *Int. J. Food Prop.*, **18**(2), 332-347. https://doi.org/10.1080/10942912.2012.693561.

ASTM (2000), ASTM D854: Standard test methods for specific gravity of soil solids by water pycnometer, ASTM International, West Conshohocken, PA, USA.

ASTM (2011), ASTM D3080/D3080 M-11: Standard test method for direct shear test of soils under consolidated drained conditions, ASTM International, West Conshohocken, PA, USA.

Bang, J.U., Lee, M., Park, D.Y., Chang, I. and Cho, G.C. (2024), "Effects of soil composition and curing conditions on the strength and durability of Cr^{3+}-crosslinked biopolymer-soil composites", *Constr. Build. Mater.*, **449**, 138440. https://doi.org/10.1016/j.conbuildmat.2024.138440.

Bang, J.U., Lee, M., Park, D.Y. and Cho, G.C. (2025), "Shear strength of crosslinked xanthan gum biopolymer treated sand-clay mixture", *Geomech. Eng.*, **41**(1), 115-127. https://doi.org/10.12989/gae.2025.41.1.115.

Baruthio, F. (1992), "Toxic effects of chromium and its compounds", *Biol. Trace Elem. Res.*, **32**(1), 145-153. https://doi.org/10.1007/BF02784599.

Casas, J.A., Santos, V.E. and García-Ochoa, F. (2000), "Xanthan gum production under several operational conditions: molecular structure and rheological properties", *Enzyme Microb. Technol.*, **26**(2), 282-291. https://doi.org/10.1016/S0141-0229(99)00160-X.

Chang, I. and Cho, G.C. (2019), "Shear strength behavior and parameters of microbial gellan gum-treated soils: from sand to clay", *Acta Geotech.*, **14**(2), 361-375. https://doi.org/10.1007/s11440-018-0641-x.

Chang, I., Cho, G.C. and An Tran, T.P. (2023), "Water-retention properties of xanthan-gum-biopolymer-treated soils", *Environ. Geotech. J.*, **11**(2), 152-163. https://doi.org/10.1680/jenge.22.00098.

Chang, I., Im, J., Prasidhi, A.K. and Cho, G.C. (2015), "Effects of xanthan gum biopolymer on soil strengthening", *Constr. Build. Mater.*, **74**, 65-72. https://doi.org/10.1016/j.conbuildmat.2014.10.026.

Chang, I., Lee, M. and Cho, G.C. (2019), "Global CO2 emission-related geotechnical engineering hazards and the mission for sustainable geotechnical engineering", *Energies*, **12**(13), 2567. https://doi.org/10.3390/en12132567.

Chantaro, P., Pongsawatmanit, R. and Nishinari, K. (2013), "Effect of heating–cooling on rheological properties of tapioca starch paste with and without xanthan gum", *Food Hydrocoll.*, **31**(2), 183-194. https://doi.org/10.1016/j.foodhyd.2012.10.026.

Chen, Z., Liu, J., Wang, Y., Qi, C., Ma, X., Che, W. and Ma, K. (2024), "Wetting–drying effects on the mechanical performance of xanthan gum biopolymer-stabilized soil", *Environ. Earth Sci.*, **83**(7), 197. https://doi.org/10.1007/s12665-024-11483-8.

Comba, S. and Sethi, R. (2009), "Stabilization of highly concentrated suspensions of iron nanoparticles using shear-thinning gels of xanthan gum", *Water Res.*, **43**(15), 3717-3726. https://doi.org/10.1016/j.watres.2009.05.046.

Dai, C., Liu, J., Mei, H., Hao, S., Song, Z., Wang, Y., Che, W., Chen, Z., Bu, F. and Wang, Z. (2023), "Investigation into xanthan gum biopolymer on mitigating cracking and erosion behavior of soil", *J. Mater. Civ. Eng.*, **35**(12), 04023460. https://doi.org/10.1061/JMCEE7.MTENG-15975.

Das, B.M. and Sivakugan, N. (2018), *Principles of foundation engineering*, Cengage learning, Boston, Massachusetts, USA.

Davisson, M. (1972), High Capacity Piles. Proc. Soil Mech. Lecture Series, Innovations in Foundation Construction. ASCE-Illinois Section.

DIN (1996), DIN 18126: Soil investigation and testing - Determination of density of non-cohesive soils for maximum and minimum compactness, Beuth publishing DIN, Germany.

Dong, J., Chen, F., Zhou, M. and Zhou, X. (2018), "Numerical analysis of the boundary effect in model tests for single pile under lateral load", *Bull. Eng. Geol. Environ.*, **77**(3), 1057-1068. https://doi.org/10.1007/s10064-017-1182-5.

Gamez, J.A. and Olson, S.M. (2022), "Compressibility-based interpretation of cone penetrometer calibration chamber tests and corresponding boundary effects", *Geotech. Test. J.*, **45**(4), 778-796. https://doi.org/10.1520/GTJ20210129.

Göttsche, K.M., Steinhagen, U. and Juhl, P.M. (2015), "Numerical evaluation of pile vibration and noise emission during offshore pile driving", *Appl. Acoust.*, **99**, 51-59. https://doi.org/10.1016/j.apacoust.2015.05.008.

Hansen, E.W. and Lund, T. (1995), "Gelation of xanthan in the presence of trivalent chromic ions monitored by proton NMR spin-lattice relaxation. A kinetic study", *J. Phys. Chem.*, **99**(24), 9811-9817. https://doi.org/10.1021/j100024a023.

Hirany, A. and Kulhawy, F. (1988), "Conduct and interpretation of load tests on drilled shaft foundations: Volume 1 detailed guidelines", Electric Power Research Inst., Palo Alto, CA (USA); Cornell University, Ithaca.

Housel, W.S. (1966), "Pile load capacity: Estimates and test results", *J. Soil Mech. Found. Div.*, **92**(SM5, Proc Paper 490), https://doi.org/10.1061/JSFEAQ.0000887.

Jerez Lazo, C., Lee, N., Tripathi, P., Joykutty, L., Jayachandran, K. and Lee, S.J. (2024), "A fungus-based soil improvement using Rhizopus oryzae inoculum", *Int. J. Geo-Eng.*, **15**(1), 18. https://doi.org/10.1186/s40703-024-00218-0.

Jiang, T., Zhao, J.D. and Zhang, J.R. (2022), "Splitting tensile strength and microstructure of xanthan gum-treated loess", *Sci. Rep.*, **12**(1), 9921. https://doi.org/10.1038/s41598-022-14058-4.

Katzbauer, B. (1998), "Properties and applications of xanthan gum", *Polym. Degrad. Stab.*, **59**(1), 81-84. https://doi.org/10.1016/S0141-3910(97)00180-8.

Kim, G.Y., Park, S. and Chang, I. (2025), "Effect of biopolymer-based soil treatment on lateral earth pressure in sandy soil backfill: An experimental study utilizing a laboratory-scale soil tank apparatus and PIV analysis", *J. Geotech. Geoenviron. Eng.*, **151**(7), 06025002. https://doi.org/10.1061/JGGEFK.GTENG-13027.

Kim, M., Park, S. and Chang, I. (2023), "Experimental study on the biopolymer hydrogel effect on pile driving rResistance", *Proceedings of the Geo-Congress 2023*, Los Angeles, March.

Kumar, A. and Sujatha, R. (2021), "Experimental investigation on the shear strength and deformation behaviour of xanthan gum and guar gum treated clayey sand", *Geomech. Eng.*, **26**(2), 101-115. https://doi.org/10.12989/gae.2021.26.2.101.

Kummar, S., Dull, N.R., Helsper, S. and Liberatore, M.W. (2025), "Effect of shear rate, temperature, and salts on the viscosity and viscoelasticity of semi-dilute and entangled xanthan gum", *J. Appl. Polym. Sci.*, **142**(3), e56372. https://doi.org/10.1002/app.56372.

Kwon, Y.M., Chang, I. and Cho, G.C. (2023a), "Xanthan biopolymer-based soil treatment effect on kaolinite clay fabric and structure using XRD analysis", *Sci. Rep.*, **13**(1), 11666. https://doi.org/10.1038/s41598-023-38844-w.

Kwon, Y.M., Moon, J.H., Cho, G.C., Kim, Y.U. and Chang, I. (2023b), "Xanthan gum biopolymer-based soil treatment as a construction material to mitigate internal erosion of earthen embankment: A field-scale", *Constr. Build. Mater.*, **389**(131716. https://doi.org/10.1016/j.conbuildmat.2023.131716.

Lee, M., Chang, I. and Cho, G.C. (2023a), "Advanced biopolymer–based soil strengthening binder with trivalent chromium–xanthan gum crosslinking for wet strength and durability enhancement", *J. Mater. Civ. Eng.*, **35**(10), 04023360. https://doi.org/10.1061/JMCEE7.MTENG-16123.

Lee, M., Chang, I., Park, D.Y. and Cho, G.C. (2023b), "Strengthening and permeability control in sand using Cr^{3+}-crosslinked xanthan gum biopolymer treatment", *Transp. Geotech.*, **43**(101122), https://doi.org/10.1016/j.trgeo.2023.101122.

Lee, M., Im, J., Cho, G.C., Ryu, H.H. and Chang, I. (2021), "Interfacial shearing behavior along xanthan gum biopolymer-treated sand and solid iInterfaces and its meaning in geotechnical engineering aspects", *Appl. Sci.*, **11**(1), 139. https://doi.org/10.3390/app11010139.

Lee, M., Kwon, Y.M., Park, D.Y., Chang, I. and Cho, G.C. (2022), "Durability and strength degradation of xanthan gum based biopolymer treated soil subjected to severe weathering cycles", *Sci. Rep.*, **12**(1), 19453. https://doi.org/10.1038/s41598-022-23823-4.

Lee, S. and Chang, I. (2025), "Inter-particle bonding mechanisms in biopolymer-hydrogel stabilized granular soils: A microscopic perspective", *Geomech. Eng.*, **41**(2), 275-285. https://doi.org/10.12989/gae.2025.41.2.275.

Lee, S., Titulaer, B., Ryu, H.H. and Chang, I. (2024), "An evaluation of the technical viability of employing combinations of xanthan gum and clay as an additive in Tunnel Boring Machine (TBM) slurries", *Geomech. Eng.*, **39**(4), 333-345. https://doi.org/10.12989/gae.2024.39.4.333.

Liu, Z. and Yao, P. (2015), "Injectable thermo-responsive hydrogel composed of xanthan gum and methylcellulose double networks with shear-thinning property", *Carbohydr. Polym.*, **132**, 490-498. https://doi.org/10.1016/j.carbpol.2015.06.013.

Lund, T., Smidsrød, O., Torger Stokke, B. and Elgsaeter, A. (1988), "Controlled gelation of xanthan by trivalent chronic ions", *Carbohydr. Polym.*, **8**(4), 245-256. https://doi.org/10.1016/0144-8617(88)90064-1.

Mali, K.K., Ghorpade, V.S., Dias, R.J. and Dhawale, S.C. (2023), "Synthesis and characterization of citric acid crosslinked carboxymethyl tamarind gum-polyvinyl alcohol hydrogel films", *Int. J. Biol. Macromol.*, **236**, 123969. https://doi.org/10.1016/j.ijbiomac.2023.123969.

Martinez, A., Dejong, J., Akin, I., Aleali, A., Arson, C., Atkinson, J., Bandini, P., Baser, T., Borela, R., Boulanger, R., Burrall, M., Chen, Y., Collins, C., Cortes, D., Dai, S., DeJong, T., Del Dottore, E., Dorgan, K., Fragaszy, R., Frost, J.D., Full, R., Ghayoomi, M., Goldman, D.I., Gravish, N., Guzman, I.L., Hambleton, J., Hawkes, E., Helms, M., Hu, D., Huang, L., Huang, S., Hunt, C., Irschick, D., Lin, H.T., Lingwall, B., Marr, A., Mazzolai, B., McInroe, B., Murthy, T., O'Hara, K., Porter, M., Sadek, S., Sanchez, M., Santamarina, C., Shao, L., Sharp, J., Stuart, H., Stutz, H.H., Summers, A., Tao, J., Tolley, M., Treers, L., Turnbull, K., Valdes, R., van Paassen, L., Viggiani, G., Wilson, D., Wu, W., Yu, X. and Zheng, J. (2021), "Bio-inspired geotechnical engineering: principles, current work, opportunities and challenges", *Geotechnique*, **72**(8), 687-705. https://doi.org/10.1680/jgeot.20.P.170.

Marudova-Zsivanovits, M., Jilov, N. and Gencheva, E. (2007), "Rheological investigation of xanthan gum–chromium gelation and its relation to enhanced oil recovery", *J. Appl. Polym. Sci.*, **103**(1), 160-166. https://doi.org/10.1002/app.25025.

Mitchell, J. and Soga, K. (2005), *Fundamentals of soil behavior*, John Wiley & Sons Ltd, Hoboken, New Jersey, USA.

Nguyen, Q.V., Fatahi, B. and Hokmabadi, A.S. (2017), "Influence of size and load-bearing mechanism of piles on seismic performance of buildings considering soil–pile–structure interaction", *Int. J. Geomech.*, **17**(7), 04017007. https://doi.org/10.1061/(ASCE)GM.1943-5622.0000869.

Park, D.Y., Chang, I., Lee, M. and Cho, G.C. (2025), "Enhancing soil liquefaction resistance and small-strain dynamic properties using cation-crosslinked biopolymer hydrogel", *Soil Dyn. Earthq. Eng.*, **190**, 109212. https://doi.org/10.1016/j.soildyn.2025.109212.

Park, S., Kim, G.Y. an d Chang, I. (2024a), "Experimental study on the effect of surface-projected conditions on the mechanical behavior of pile embedded in sand", *Int. J. Geo-Eng.*, **15**(1), 22. https://doi.org/10.1186/s40703-024-00223-3.

Park, S., Yum, J.H., Lee, M., Cho, G.C., Lee, S. and Chang, I. (2024b), "Bioinspired biopolymer hydrogel application to improve installation efficiency and load carrying capacity of piles", *Proceedings of the Geo-Congress 2024*, Vancouver, Canada, February.

Prud'homme, R.K., Uhl, J.T., Poinsatte, J.P. and Halverson, F. (1983), "Rheological monitoring of the formation of polyacrylamide/Cr^{+3} gels", *Soc. Pet. Eng. J.*, **23**(5), 804-808. https://doi.org/10.2118/10948-PA.

Quanjie, C., Shantong, L., Yijie, W., Yihua, G., Bo, W., Chen, G. and Yongkang, K. (2024), "Research review on the influence of hammering pile vibration on the surrounding environment", *Proceedings of the 2024 7th International Symposium on Traffic Transportation and Civil Architecture (ISTTCA 2024)*, Tianjin, China, June.

Shibaev, A.V., Muravlev, D.A., Muravleva, A.K., Matveev, V.V., Chalykh, A.E. and Philippova, O.E. (2020), "pH-dependent gelation of a stiff anionic polysaccharide in the presence of metal ions", *Polymers*, **12**(4), 868. https://doi.org/10.3390/polym12040868.

Sierra, K., An, J., Shamet, R., Chen, J., Kim, Y.J., Nam, B.H. and Park, P. (2024), "A review of geopolymer binder as a grouting material", *Int. J. Geo-Eng.*, **15**(1), 21. https://doi.org/10.1186/s40703-024-00221-5.

Stokes, J.R., Macakova, L., Chojnicka-Paszun, A., de Kruif, C.G. and de Jongh, H.H.J. (2011), "Lubrication, adsorption, and rheology of aqueous polysaccharide solutions", *Langmuir*, **27**(7), 3474-3484. https://doi.org/10.1021/la104040d.

Tran, T.P.A., Chang, I. and Cho, G.C. (2019), "Soil water retention and vegetation survivability improvement using microbial biopolymers in drylands", *Geomech. Eng.*, **17**(5), 475-483. https://doi.org/10.12989/gae.2019.17.5.475.

Vesić, A.S. (1963), "Bearing capacity of deep foundations in sand", *Highway Research Record*, **39**(39), 112-153.

Wan, J., Ouyang, F., Xiao, H., Wang, L. and Tao, G. (2024), "Experimental study on the physical and mechanical properties of modified clay using xanthan gum and guar gum composite materials", *Sustainability*, **16**(13), 5432. https://doi.org/10.3390/su16135432.

Weng, Z., Wang, L., Liu, Q., Pan, X., Xu, Y. and Li, J. (2021), "Improving the unconfined compressive strength of red clay by combining biopolymers with fibers", *J. Renew. Mater.*, **9**(8), 1503-1517. https://doi.org/10.32604/jrm.2021.015003.

Zhang, W., Huang, R., Xiang, J. and Zhang, N. (2024), "Recent advances in bio-inspired geotechnics: From burrowing strategy to underground structures", *Gondwana Res.*, **130**, 1-17. https://doi.org/10.1016/j.gr.2023.12.018.

Zhang, W., Xiang, J., Huang, R. and Liu, H. (2023), "A review of bio-inspired geotechnics-perspectives from geomaterials, geo-components, and drilling & excavation strategies", *Biogeotech.*, **1**(3), 100025. https://doi.org/10.1016/j.bgtech.2023.100025.

Zhang, X., Cao, W. and Zhang, X. (2024), "Experimental study on mechanical and hydraulic properties of xanthan gum improved low liquid limit silty soil", *Sci. Rep.*, **14**(1), 11072. https://doi.org/10.1038/s41598-024-61875-w.

Zhong, L., Oostrom, M., Truex, M.J., Vermeul, V.R. and Szecsody, J.E. (2013), "Rheological behavior of xanthan gum solution related to shear thinning fluid delivery for subsurface remediation", *J. Hazard. Mater.*, **244-245**, 160-170. https://doi.org/10.1016/j.jhazmat.2012.11.028.

Zivari, A., Siavoshnia, M. and Rezaei, H. (2023), "Effect of lime-rice husk ash on geotechnical properties of loess soil in Golestan province, Iran", *Int. J. Geo-Eng.*, **14**(1), 20. https://doi.org/10.1186/s40703-023-00199-6.

CC